Supporting Information
for

Static-dynamic vacancies via pre-embedded heterogeneous Gd ions in RuO_2/Gd-Co_3O_4 enabling robust water oxidation

Xinhua Li [#a], Honghao Zhong [#a], Shen Cheng [b], Wanchuan Jin [a], Yuxin Wang [a], Yuanhong Liu [a], Qinghua Liu [b], Ruishi Xie *[a], Yuanli Li *[a]

[a] Innovation Center of Nuclear Environmental Safety Technology, School of Materials and Chemistry, Analytical and Testing Center, Southwest University of Science and Technology, Mianyang 621010, Sichuan, P. R. China
[b] National Synchrotron Radiation Laboratory, University of Science and Technology of China, Hefei 230029, Anhui, P. R. China

[#] These authors contributed equally to this work.
*Email: yli@swust.edu.cn, rxie@swust.edu.cn

Physical characterizations

Scanning electron microscopy (SEM) images was collected by a Field Emission Scanning Electron microscope (FESEM Zeiss Ultra-55) at an acceleration voltage of 10 kV. Transmission electron microscopy (TEM) and energy dispersive X-ray spectroscopy (EDS) images were recorded on a JEM 2100F at an acceleration voltage of 200 kV. X-ray diffraction (XRD) patterns were recorded by a Bruker D8 Advance A25 XRD diffractometer with Cu Kα radiation (λ = 1.5405 Å) at a scan rate of 5° min^{-1} in the 2θ range of 10° ~ 80°. X-ray photoelectron spectroscopy (XPS) analysis was conducted on a Thermo Scientific Escalab250Xi spectroscope with Al-Kα radiation. The collected XPS spectra was calibrated by referencing the binding energy of C 1s to 284.80 eV. Raman spectra were collected on a Renishaw inVia confocal Raman microscope under an excitation of 532 nm laser with the power of 4.0 mW. Electron paramagnetic resonance (EPR) was measured on a Bruker A300 spectrometer. The mass loading of materials was measured by an Agilent 730 inductively coupled plasma optical emission spectrometry (ICP-OES). The leaching rates of metal ions were determined using an Agilent 7850 inductively coupled plasma mass spectrometer (ICP-MS) for quantitative analysis.

Electrochemical tests

Three-electrode system on a CHI 760e electrochemical workstation (Chenhua, Shanghai) in a 0.5 M H_2SO_4 solution at ambient temperature. The catalysts self-supported on CC (1 cm × 1 cm), a Pt sheet (1 cm × 1 cm) and a saturated Hg/Hg_2SO_4 electrode were used as the working, counter, and reference electrodes, respectively. Before tests, the potential of the Hg/Hg_2SO_4 reference electrode was calibrated in H_2-saturated 0.5 M H_2SO_4 solution using Pt mesh as both working and counter electrode.[1] As shown in Figure S5, The CV curve were recorded at a scan rate of 1 mV/s. The potential achieved at the zero current is the thermodynamic potential for H_2 evolution/oxidation. The zero current was achieved at -0.708 V vs. Hg/Hg_2SO_4, and therefore $E_{RHE} = E_{Hg/Hg^2SO^4} + 0.708$ V. CV tests at 50 mV s^{-1} were then conducted to remove impurities from the electrode surface. The LSV curves were then recorded at a scan rate of 2 mV s^{-1} in 0.5 M H_2SO_4. All the potentials reported in this work were corrected by ohmic loss according to the following equation.

$$E_{iR\text{-}free} = E_{raw} - iR_s$$

where $E_{iR\text{-}free}$, E_{raw}, i and R_s represent the corrected potential, raw potential, current and solution resistance, respectively.

Tafel plots were transferred from LSV curves according to the following equation.

$$\eta = a + b * \log j$$

where η denotes the overpotential, j is the current density and b is the Tafel slope.

The OER kinetics was investigated using EIS at a potential of 1.43 V vs. RHE, within the frequency range of 0.01-100 kHz and an amplitude of 5 mV. Long-term chronopotentiometry measurements were conducted at a benchmark current density of 10 mA $cm^{-2}$and 100 mA cm^{-2}. The C_{dl} was obtained by applying a linear fit to plots of current density difference versus sweep rate, where the slope represents the C_{dl} value. The ECSA of the measured electrocatalysts was calculated using a conventional CV method, in which the current density was recorded upon a voltage increase from 2 to 10 mV with a sweep rate of 2 mV s^{-1} within a voltage window of 1.07 - 1.17 V vs. RHE and in the absence of Faradaic processes.

In situ EIS measurements

In situ EIS measurements were performed over a frequency range from 10^{-2} to 10^{5} Hz with AC amplitude of 5 mV.

In situ SRIR measurements

In situ SRIR measurements were conducted at the infrared beamline BL01B of NSRL using a homemade top-plate cell reflection IR setup with a ZnSe crystal as the infrared transmission window. The catalyst electrode was pressed tightly against the ZnSe crystal window with a micron-scale gap to minimize the loss of infrared light. To ensure high-quality SRIR spectra, the apparatus utilized a reflection mode with a vertical incidence of infrared light. The infrared spectrum was obtained by averaging 128 scans at a resolution of 4 cm^{-1}. Prior to each systemic OER measurement, the background spectrum of the catalyst electrode was obtained at an open-circuit voltage. The test potential range of RuO_2/Gd-Co_3O_4 was measured from 1.2 V to 1.8 V vs. RHE, with a measurement interval of 0.1 V. For Co_3O_4, the range was from 1.5 V to 2.1 V, and for Gd-Co_3O_4, it was from 1.5 V to 2.0 V. The infrared data was processed and smoothed using OPUS software.

Supplementary figures

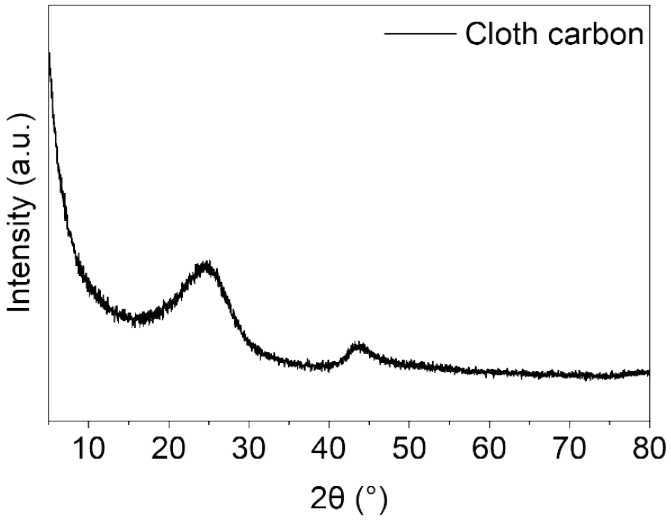

Figure S1. XRD pattern of the CC substrate.

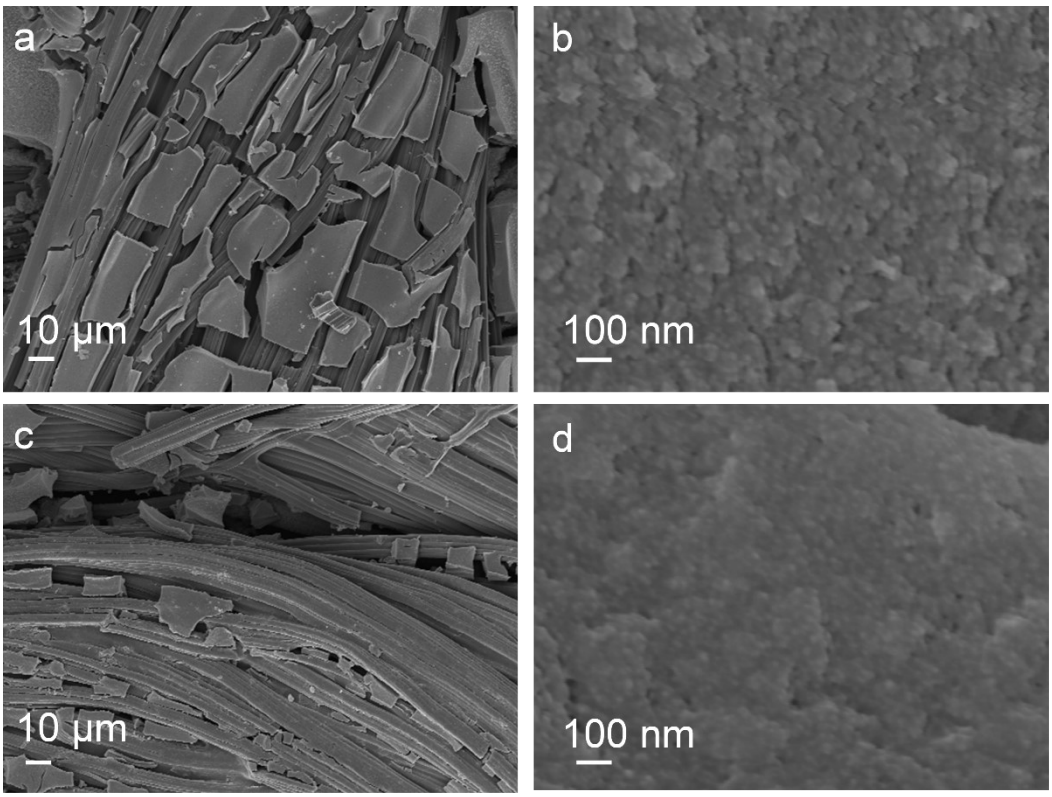

Figure S2. SEM images of (a, b) Gd-Co_3O_4 and (c, d) RuO_2/Gd-Co_3O_4.

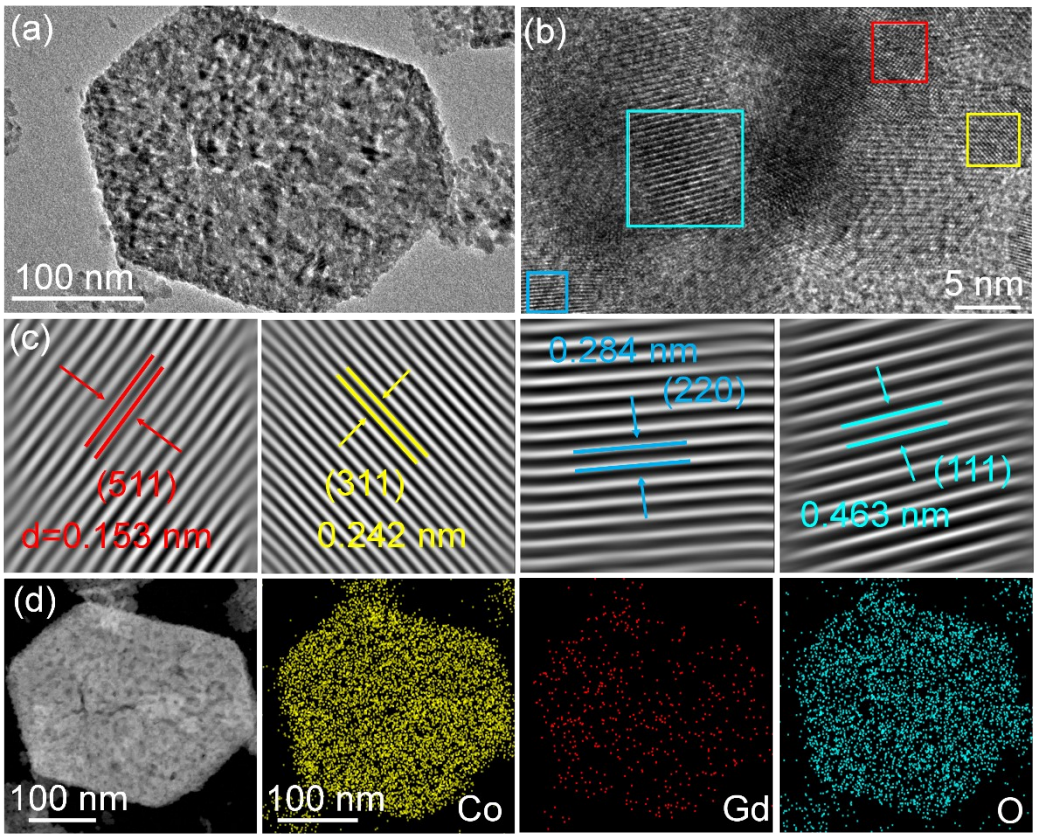

Figure S3. (a) TEM image, (b) HRTEM image, (c) IFFT graphs of the Gd-Co_3O_4 (below), (d) STEM image and corresponding element mapping images of Gd-Co_3O_4.

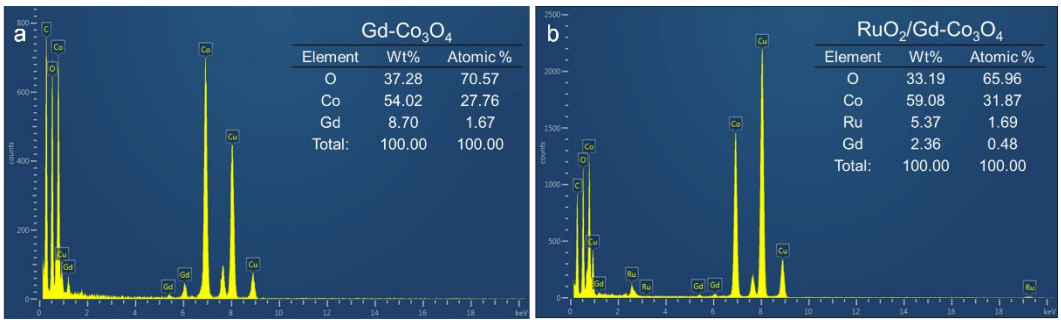

Figure S4. EDS patterns of (a) Gd-Co_3O_4 and (b) RuO_2/Gd-Co_3O_4.

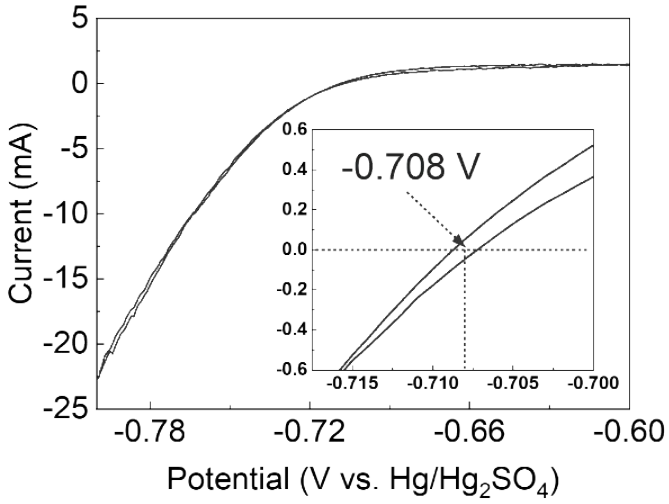

Figure S5. Hg/Hg_2SO_4 reference electrode calibration in H_2-saturated 0.5 M H_2SO_4 solution.

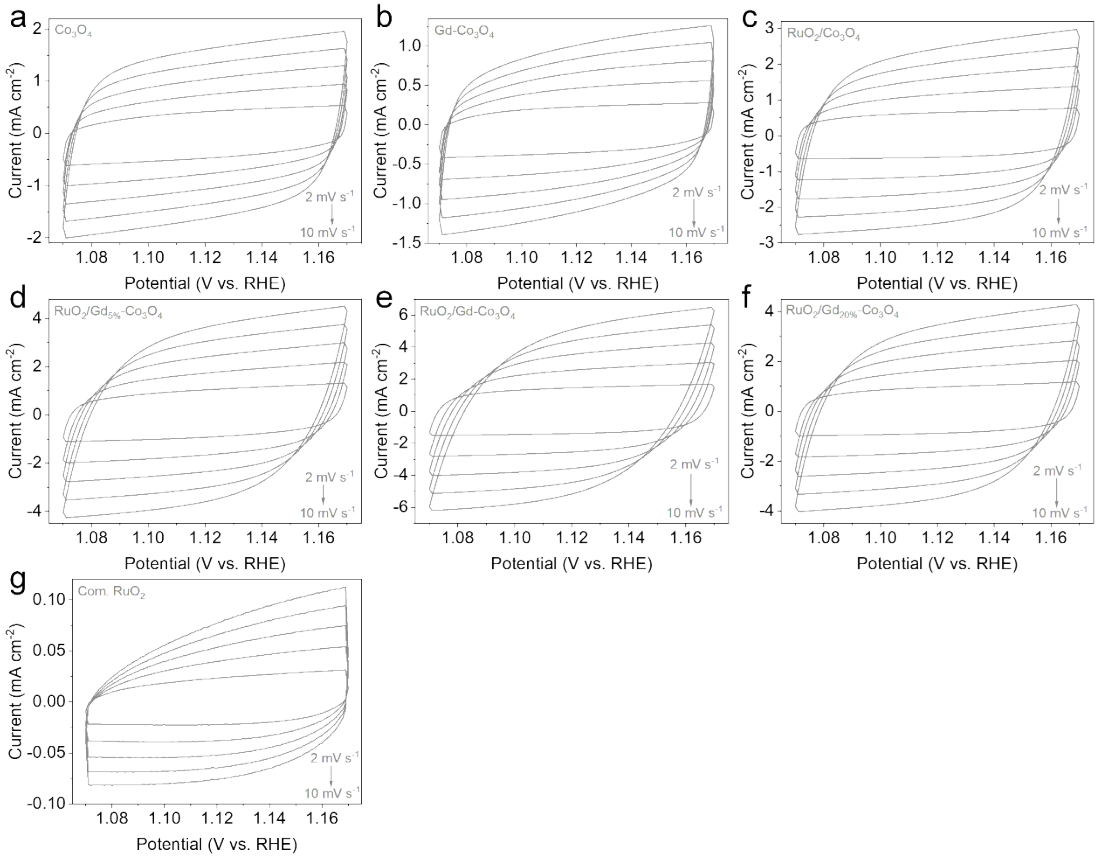

Figure S6. ECSA determination. CV plots of (a) Co_3O_4, (b) Gd-Co_3O_4, (c) RuO_2/ Co_3O_4, (d) $RuO_2/Gd_{5\%}$-Co_3O_4, (e) RuO_2/Gd-Co_3O_4, (f) $RuO_2/Gd_{20\%}$-Co_3O_4 and (d) Com. RuO_2, respectively, at different scan rates.

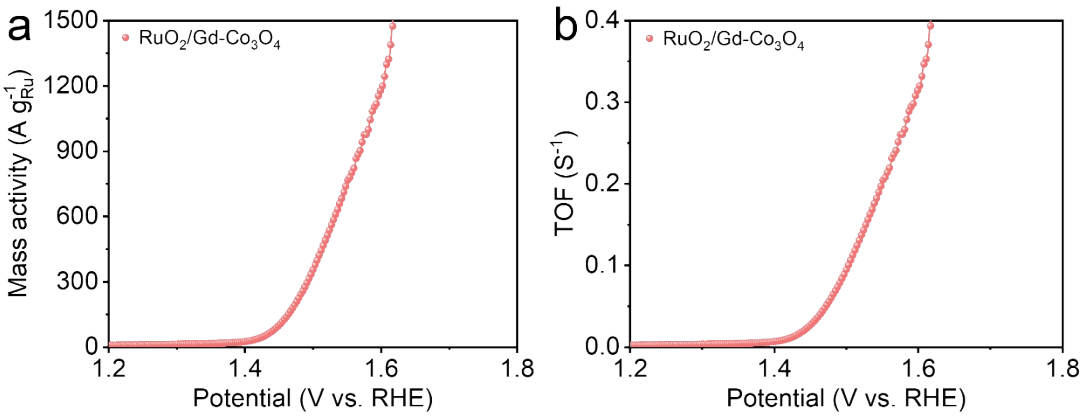

Figure S7. (a) Turnover frequency (TOF) and (b) mass activity of RuO_2/Gd-Co_3O_4.

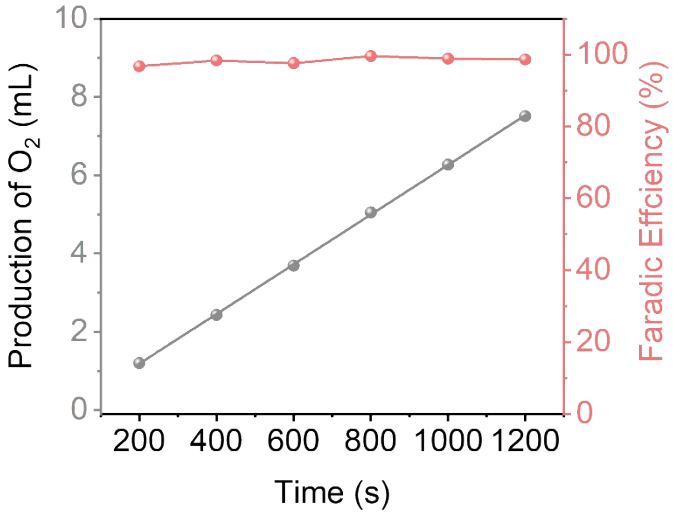

Figure S8. Faradaic efficiency of the RuO_2/Gd-Co_3O_4 catalyst during the OER.

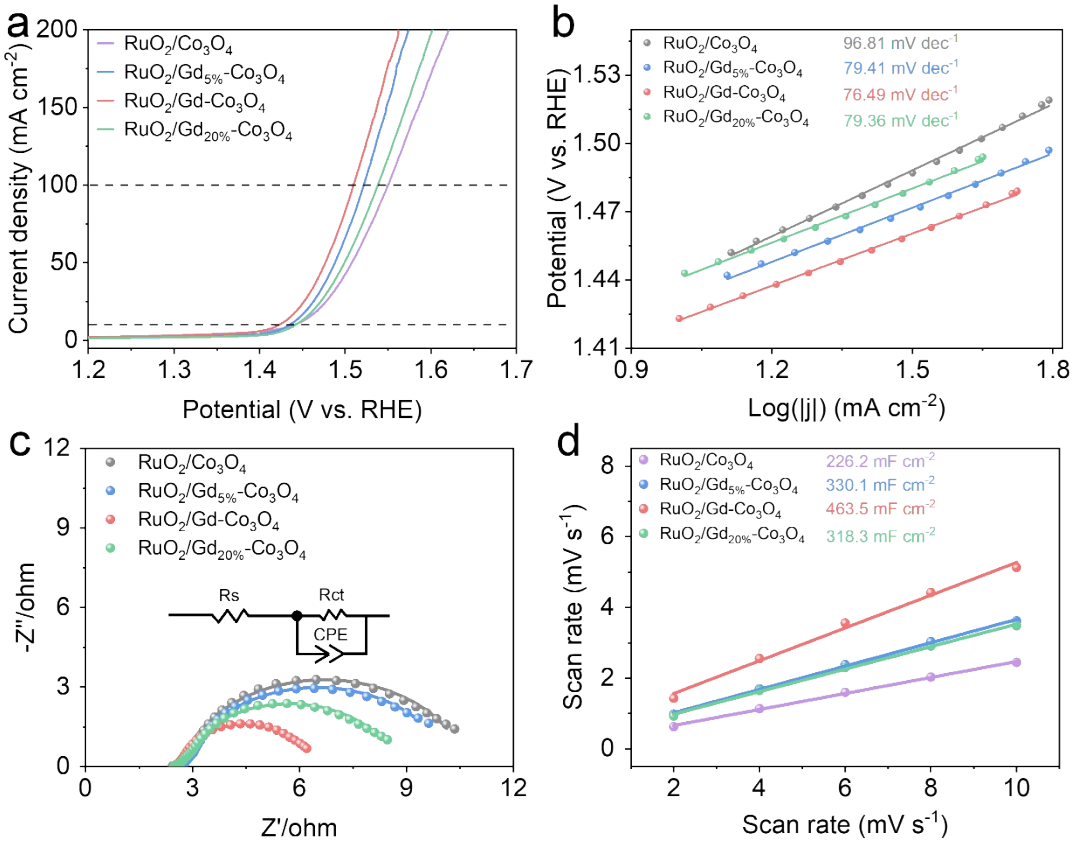

Figure S9. (a) LSV curves, (b) Tafel plots, (c) EIS and (d) C_{dl} measurements for RuO_2/Gd-Co_3O_4 with varying Gd concentrations.

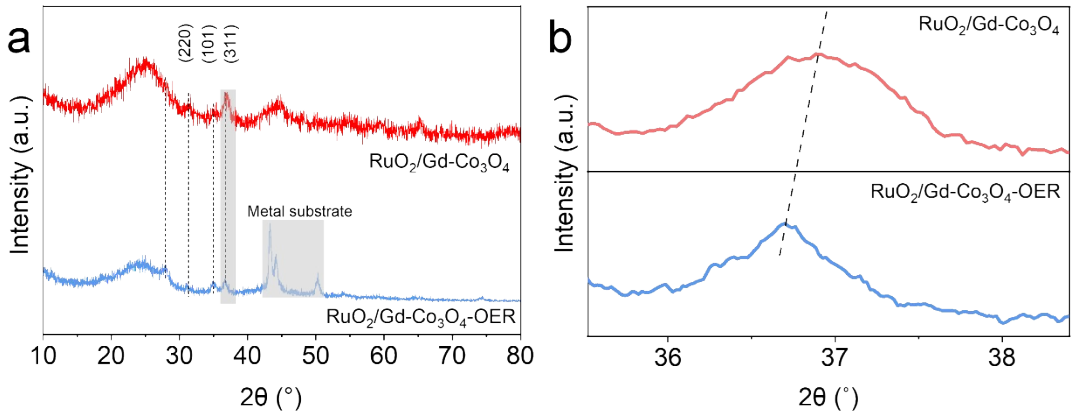

Figure S10. (a) XRD patterns and (b) partial magnification of RuO_2/Gd-Co_3O_4 before and after the chronopotentiometry test.

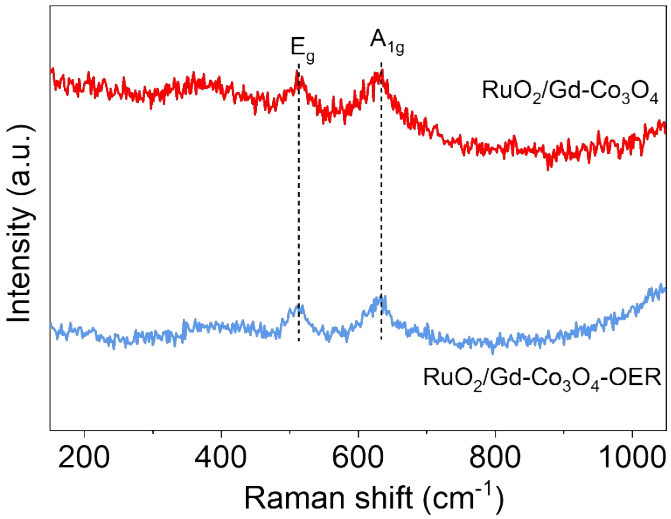

Figure S11. Raman patterns of the RuO_2/Gd-Co_3O_4 before and after the chronopotentiometry test.

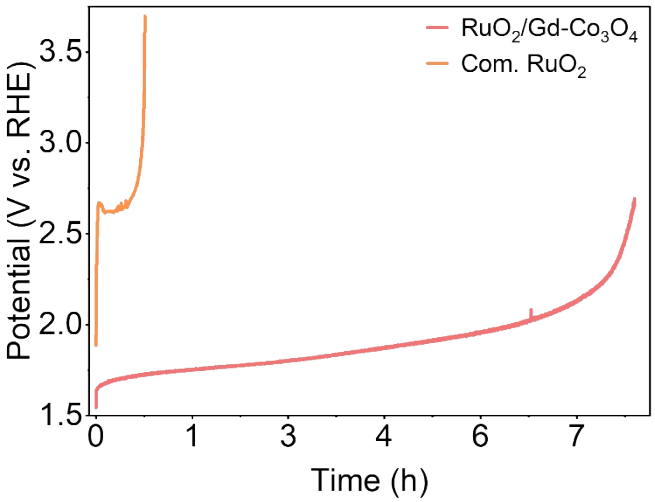

Figure S12. Chronoamperometric stability tests of RuO_2/Gd-Co_3O_4 and Com. RuO_2 at 100 mA cm^{-2}.

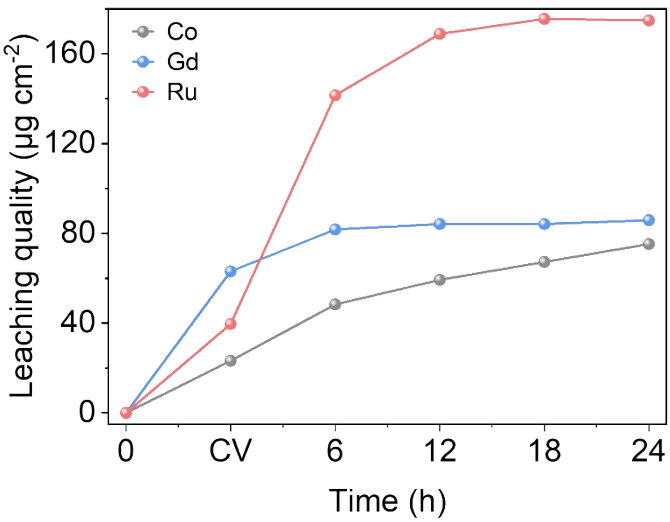

Figure S13. Cumulative leaching of Gd ions from RuO_2/Gd-Co_3O_4 measured at a constant current density of 10 mA cm^{-2} over varying electrolysis durations.

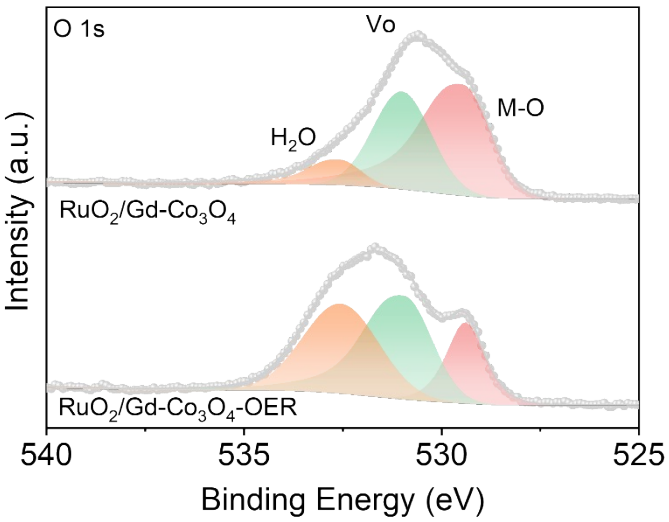

Figure S14. The O1s XPS spectra of RuO_2/Gd-Co_3O_4 before and after the chronopotentiometry test.

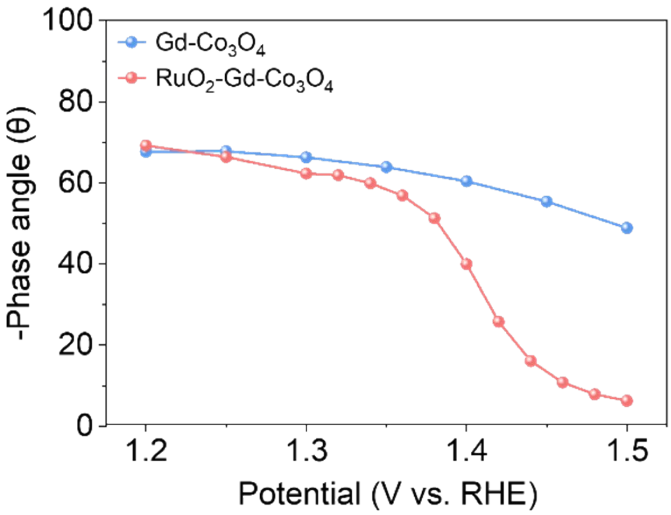

Figure S15. The corresponding phase peak angles of Gd-Co_3O_4 and RuO_2/Gd-Co_3O_4 from 1.20 to 1.50 V vs. RHE.

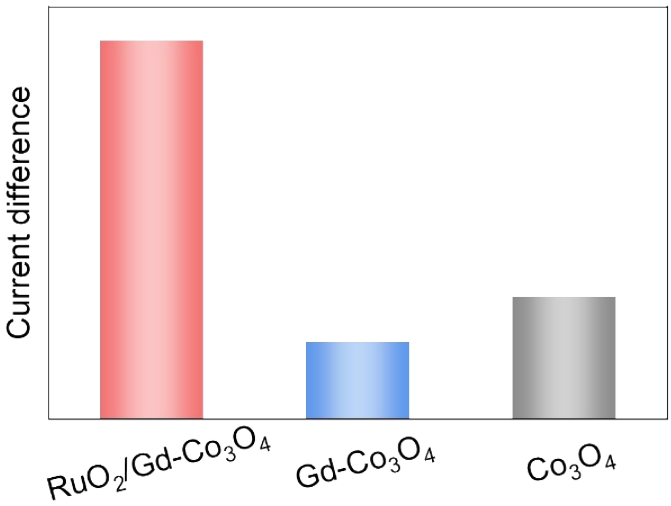

Figure S16. The current differences of the polarization curves of Co_3O_4, Gd-Co_3O_4 and RuO_2/Gd-Co_3O_4 in 0.5 M H_2SO_4 solution with and without 1.0 M methanol.

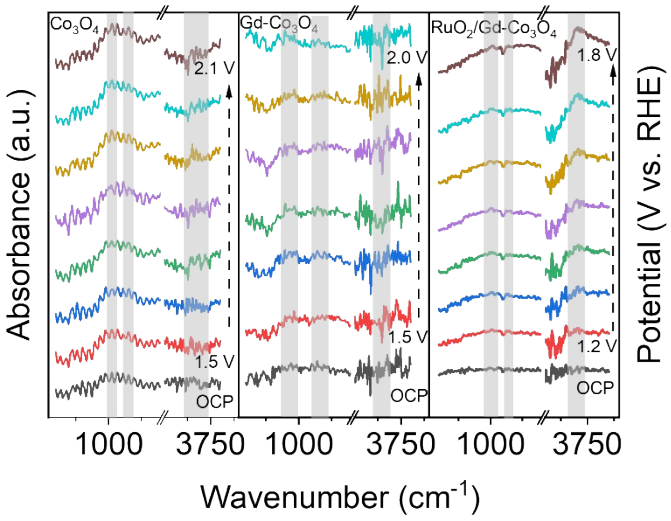

Figure S17. Original SRIR spectra for Co_3O_4, Gd-Co_3O_4, and RuO_2/Gd-Co_3O_4.

Supplementary Table

Table S1. EIS fitting results of the Co_3O_4, Gd-Co_3O_4, RuO_2/Gd-Co_3O_4 with varying Gd concentrations and Com. RuO_2.

Electrode	Rs (Ω)	CPE (F cm^{-2})	Rct (Ω)
Co_3O_4	2.629	0.181	136.6
Gd-Co_3O_4	2.642	0.124	121.6
RuO_2/Co_3O_4	2.672	0.282	8.056
RuO_2/$Gd_{5\%}$-Co_3O_4	2.753	0.400	7.504
RuO_2/Gd-Co_3O_4	2.605	0.629	3.783
RuO_2/$Gd_{20\%}$-Co_3O_4	2.634	0.346	6.149
Com. RuO_2	2.681	0.00935	557

Table S2. Comparison of OER activities, stabilities, and mass activities of various electrocatalysts in acidic conditions.

Catalysts	Electrolyte	Overpotential (η_{10}: mV)	Stability (η_{10}: h)	Mass activity (A g_{Ru}^{-1}@V vs. RHE)	Ref.

RuO_2/Gd-Co_3O_4	0.5 M H_2SO_4	193	72	585.774 @1.53	This work
Mn-Ru@RuO_2	0.5 M H_2SO_4	220	220	1370 @1.53	[2]
RuCo@C/CC	0.5 M H_2SO_4	200	25	200 @1.48	[3]
Mn-RuO_2/CeO_2	0.1 M $HClO_4$	227	300	-	[4]
6% Sm-RuO_2	0.1 M $HClO_4$	218.5	130	-	[5]
RuO_2/Ru	0.1 M $HClO_4$	245	100	-	[6]
Cr_2O_3/RuO_2	0.5 M H_2SO_4	220	100	-	[7]
AC-Sm-RuO_2	0.5 M H_2SO_4	200	300	-	[8]
Ir-RuO_x@WO_3	0.1 M H_2SO_4	148	12	-	[9]
Ru@La/Co_3O_4-20	0.5 M H_2SO_4	244	30	-	[10]
C-Ru-Co_3O_4	0.5 M H_2SO_4	252	30	-	[11]
$Ru_{0.20}$(Ir,Fe,Co, Ni)$_{0.80}$	0.1 M $HClO_4$	237	24	92@1.53	[12]
Ru-NiFe-BDC/NF	0.5 M H_2SO_4	247	20	66.6 @1.5	[13]
Ru/RuO_2-Co_3O_4	0.1 M $HClO_4$	226	19	-	[14]
Co_3O_4/RuO_2	0.5 M H_2SO_4	257	100	-	[15]
Ru-Co_3O_4	0.5 M H_2SO_4	365	16	-	[16]
Ru_x/RuO_2	0.5 M H_2SO_4	176.7	20	-	[17]
Ru/RuO_2/NC	0.5 M H_2SO_4	211	100	-	[18]
$Ru_{0.6}Mo_{0.2}Cr_{0.2}O_x$	0.5 M H_2SO_4	204	60	577.8 @1.5	[19]
RuO_xSe_y-800	0.5 M H_2SO_4	211	18	239.1 @1.53	[20]
SiO_x/$RuCoO_x$ NPs	0.5 M H_2SO_4	217	12	-	[21]
RuO_2/D-Co_3O_4/CC	0.5 M H_2SO_4	181	120	-	[22]

References

1. W. J. Zhu, F. Yao, K. J. Cheng, M. T. Zhao, C. J. Yang, C. L. Dong, Q. M. Hong, Q. Jiang, Z. C. Wang and H. F. Liang, Direct dioxygen radical coupling driven by octahedral ruthenium-oxygen-cobalt collaborative coordination for acidic oxygen evolution reaction, *J. Am. Chem. Soc.*, 2023, **145**, 17995-18006.
2. Y. Zhang, Y. X. Li, H. H. Wei, Q. Wang, Z. X. Su, Z. X. Li, Y. Y. Gao, Y. Shen, H. Li, L. T. Zhang, D. Zu, H. F. Wang and X. Q. Gong, Efficient and durable OER electrocatalysts through vacancy engineering and core-shell structure design in acidic environment, *Mater. Today Energy*, 2024, **46**, 101722.
3. H. R. Cai, N. Jiang, L. F. Xiong, F. F. Shang, J. Hou, Y. Lin, C. Li, X. J. Zhang, D. Su and S. C. Yang, Self-supported porous carbon decorated with coralline RuCo alloy for efficient OER in acid, *Int. J. Hydrogen Energy*, 2024, **84**, 840-847.
4. J. Li, Y. T. Liu, M. Q. Yao, S. Geng and F. Liu, Enhancement of acidic OER performance through heterojunction interface coupling promoted by heteroatom

doping, *Chem. Eng. J.*, 2025, **521**, 167203.
5. W. R. Yang, J. T. Guo, X. Xie, C. L. Yang and S. Geng, Ru-O-Sm structure enhances water adsorption to improve OER performance in acidic media, *J. Electroanal. Chem.*, 2025, **996**, 119407.
6. J. H. Ni, Y. S. Han, X. Xie, C. L. Yang and S. Geng, Electrospinning-controlled calcination conditions fabrication of RuO_2/Ru nanofibers for acidic OER, *Mol. Catal.*, 2025, **586**, 115418.
7. J. Y. Zhao, N. Yao and W. Luo, Cr_2O_3/RuO_2 heterojunction catalysts for enhanced oxygen evolution reaction in acidic media, *ChemistrySelect*, 2025, **10**, e01065.
8. Y. F. Chen, Z. J. Li, H. Jang, Z. Wang, M. G. Kim, Q. Qin and X. E. Liu, Sm-induced symmetry-broken ru centers for boosting acidic water oxidation, *ACS Sustainable Chem. Eng.*, 2024, **12**, 5884-5892.
9. X. Y. Li, Z. H. Gu, J. F. Cheng, G. Z. Zhang, F. H. Zheng, J. W. Huang, J. X. Xu, G. H. Wei and J. L. Zhang, Ir-RuO_x nanoparticles on WO_3 ultrafine nanowires as catalysts for the oxygen evolution reaction in acidic media, *ACS Appl. Nano Mater.*, 2024, **7**, 12958-12969.
10. C. H. Li, C. Z. Yuan, C. L. Zhou, X. Yang, R. L. Xu, F. L. Wu, L. Xin, L. X. Wang, X. M. Zhang, K. N. Hui, S. F. Ye and Y. F. Chen, Stabilizing Ru single atoms on asymmetric La/Co_3O_4 supports with strong metal-support interaction for efficient acidic water oxidation, *ACS Catal.*, 2025, **15**, 7403-7413.
11. T. H. Liu, J. Y. Guo, A. P. Wu, Y. Y. Fan, Y. Xie and C. G. Tian, Carbon-encapsulated Ru-Co_3O_4 nanosheets as electrocatalysts for acidic water oxidation, *ACS Appl. Nano Mater.*, 2024, **7**, 13298-13307.
12. A. L. Maulana, S. Han, Y. Shan, P. C. Chen, C. Lizandara Pueyo, S. De, K. Schierle Arndt and P. Yang, Stabilizing Ru in multicomponent alloy as acidic oxygen evolution catalysts with machine learning-enabled structural insights and screening, *J. Am. Chem. Soc.*, 2025, **147**, 10268-10278.
13. P. Vijayakumar, S. Lenus, K. Pradeeswari, M. Kumar, J. H. Chang, M. Kandasamy, M. Krishnamachari, Z. F. Dai, A. A. Al-Kahtani and P. Sankar Krishnan, In situ reconstructed layered double hydroxides via MOF engineering and Ru doping for decoupled acidic water oxidation enhancement, *Energy Fuels*, 2024, **38**, 4504-4515.
14. T. T. Wang, Z. J. Li, H. Jang, M. G. Kim, Q. Qin and X. E. Liu, Interface engineering of oxygen vacancy-enriched Ru/RuO_2-Co_3O_4 heterojunction for efficient oxygen evolution reaction in acidic media, *ACS Sustainable Chem. Eng.*, 2023, **11**, 5155-5163.
15. M. T. Zhao and H. F. Liang, Crystal facet regulation and ru incorporation of Co_3O_4 for acidic oxygen evolution reaction electrocatalysis, *ACS Nanosci. Au*, 2024, **4**, 409-415.
16. R. Madhu, A. Karmakar, P. Arunachalam, J. Muthukumar, P. Gudlur and S. Kundu, Regulating the selective adsorption of OH* over the equatorial position of Co_3O_4 via doping of Ru ions for efficient water oxidation reaction, *J. Mater. Chem. A*, 2023, **11**, 21767-21779.
17. X. Y. Zhu, M. H. Fang, S. R. Ke, B. Z. Yang, S. J. Yang, Y. H. Li, M. L. Zhan and

X. Min, Rapid synthesis of an aluminum-doped ultrathin Ru_x-RuO_2 heterostructure optimized through combined wet-dry microwave radiation for efficient acidic and alkaline overall water splitting, *J. Mater. Chem. A*, 2025, **13**, 5091-5105.

18. M. Wu, Y. Y. Fan, Y. Huang, D. X. Wang, Y. Xie, A. P. Wu and C. G. Tian, Synergistic Ru/RuO_2 heterojunctions stabilized by carbon coating as efficient and stable bifunctional electrocatalysts for acidic overall water splitting, *Nano Res.*, 2024, **17**, 6931-6939.
19. J. Yang, Y. W. Zhang and Y. P. Liu, Constructing crystalline-amorphous heterophase interfaces through Cr/Mo Co-doping in RuO_2 enables efficient acidic oxygen evolution reaction, *Ionics.*, 2025, DOI: **10.1007/s11581-025-06485-w**.
20. P. Du, C. L. Lin, X. He, Z. C. Zheng, X. Y. Xie, K. Huang, M. Lei and H. L. Tang, Controlled fabrication of Ru-O-Se composites for enhanced acidic oxygen evolution, *Adv. Compos. Hybrid Mater.*, 2023, **6**, 40.
21. T. Zhu, Y. H. Wang, T. Sun, Y. C. Pi, X. D. Pi, J. Xu and K. J. Chen, d-orbital charge density regulation of SiO_x/$RuCoO_x$ nanoparticles to boost water splitting in acidic media, *Rare Met.*, 2025, **44**, 6223-6231.
22. Y. J. Liu, Z. S. Yuan, Q. Song, T. G. Xu, G. He, H. X. Sun, Q. Qiao, X. F. Guan, T. Xu, X. P. Dai and X. Zhang, Dual-defective-engineered RuO_2/D-Co_3O_4/CC composite as efficient electrocatalysts for triggering oxygen evolution reaction in acidic media, *Sci. China Mater.*, 2024, **67**, 771-779.